Paper presented at the SPIE Medical Imaging meeting, Ultrasonic Imaging and Signal Processing, 2002:

Virtual Ultrasound Sources in High-resolution Ultrasound Imaging.

Svetoslav Ivanov Nikolov, and Jørgen Arendt Jensen,
Center for Fast Ultrasound Imaging,
Ørsted•DTU, Bldg. 348,
Technical University of Denmark,
DK-2800 Lyngby, Denmark

Proceedings of SPIE, Eds. M. F. Insana and W. Walker, 2002.

```
@inbook{ref_nikolov_jensen_2002a,
  title     = "Virtual ultrasound sources in high-resolution ultrasound imaging",
  author    = "Nikolov, Svetoslav Ivanov and Jensen, {Jørgen Arendt}",
  year      = "2002",
  pages     = "395-405",
  booktitle = "Proc. SPIE - Progress in biomedical optics and imaging",
}
```

Virtual Ultrasound Sources in High-resolution Ultrasound Imaging.

Svetoslav I. Nikolov and Jørgen A. Jensen

[a] Center for Fast Ultrasound Imaging, Ørsted•DTU, Bldg 348,
Technical University of Denmark, DK-2800, Denmark

ABSTRACT

This paper investigates the concept of virtual source elements. It suggests a common framework for increasing the resolution, and penetration depth of several imaging modalities by applying synthetic aperture focusing (SAF). SAF is used either as a post focusing procedure on the beamformed data, or directly on the raw signals from the transducer elements. Both approaches increase the resolution.

The paper shows that in one imaging situation, there can co-exist different virtual sources for the same scan line - one in the azimuth plane, and another in the elevation. This property is used in a two stage beamforming procedure for 3D ultrasound imaging.

The position of the virtual source, and the created waveform are investigated with simulation, and with pulse-echo measurements. There is good agreement between the estimated wavefront and the theoretically fitted one.

Several examples of the use of virtual source elements are considered. Using SAF on data acquired for a conventional linear array imaging improves the penetration depth for the particular imaging situation from 80 to 110 mm.

The independent use of virtual source elements in the elevation plane decreases the respective size of the point spread function at 100 mm below the transducer from 7mm to 2 mm.

Keywords: synthetic aperture, ultrasound, focusing, imaging, virtual sources

1. VIRTUAL SOURCES

Focusing is done by coherently adding the responses of the individual transducer elements coming from the focal point. The coherent summation is usually done by picking up the signal in the sum, based on the round trip propagation time of the emitted pressure wave to the focal point and back to the transducer element. In order to determine the propagation time, it is necessary to create a waveform with a known shape of the wavefront, such as a spherical/cylindrical wave, and trace its propagation to a source point. If the source point coincides with an element of a transducer array, then the source is real, otherwise it is virtual. Knowing the position of the source of the spherical wave, it is possible to use synthetic aperture focusing on the received signals to achieve almost dynamic focusing in transmit and receive. The introduction of virtual ultrasound sources is, thus, a method for introducing synthetic aperture focusing in all types of images, and the purpose of this paper is to demonstrate that this can be done for all imaging modalities, and that it can yield significant increases in resolution and depth of penetration.

The use of a virtual source, created by a focused single element transducer with a circular footprint, for synthetic aperture focusing (SAF) was studied by Pasmann and Ermert,[1,2] and by Frazier and O'Brien.[3] They showed that the virtual source coincides with the fixed focal point of the transducer, and that a depth independent resolution can be achieved by using SAF. Such a configuration is shown in Fig. 1. The wavefront before the focus can be approximated with a converging spherical wave, and after the focal point as a diverging spherical

Further author information: (Send correspondence to Nikolov S. I.)
Nikolov S. I.: http://www.linkedin.com/in/svetoslavnikolov

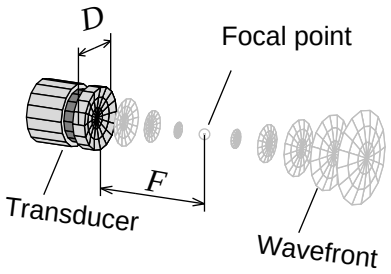

Figure 1. Virtual source created by a single element focused transducer.

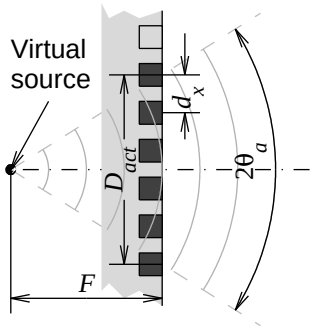

Figure 2. Virtual source in the back of the linear array.

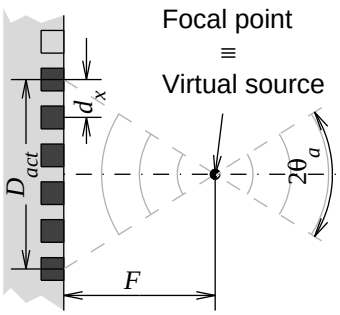

Figure 3. Virtual source in front of the linear array.

wave. For strongly focused transducers ($f_\# = F/D \sim 1,\ 1.5$), the angle of divergence θ_a, within whose limits the wavefront is a part of a sphere, can be determined by simple geometrical relations:

$$\theta_a = 2 \arctan \frac{D}{2F}, \tag{1}$$

where D is the diameter of the transducer and F is the distance to the focus. The data acquisition was done by translating the transducer along the surface at discrete steps. At every position a scan line was acquired. Then a synthetic aperture focusing (SAF) was applied on the recorded signals in order to increase the resolution. This type of SAF is known as mono-static SAF. This case is very favorable for the concept of the virtual source, because there is only one focal point, and there is no ambiguity in the position of the source.

In the following sections we will consider the position of the virtual source in the azimuth and in elevation planes for a transducer *array*, which is a more complicated case, since the focus in azimuth generally differs from the focus in the elevation.

1.1 In the Azimuth Plane

Two cases for the position of the virtual source in the elevation plane are possible, in the back or in front of the transducer, as shown in Fig. 2 and 3, respectively. The former is used for synthetic aperture ultrasound (SAU) imaging.[4–7] The purpose is to increase the signal to noise ratio (SNR) by using multiple elements in transmit, without loosing resolution. The delays τ_i applied on the elements i are:

$$\tau_i = \frac{1}{c}\left(-F + \sqrt{F^2 + \left((i-1)d_x - D_{act}/2\right)^2}\right) \tag{2}$$

$$i \in [1, N_{act}] \tag{3}$$

$$D_{act} = (N_{act} - 1)d_x,$$

where N_{act} is the number of active elements in transmit, D_{act} is the size of active aperture, and d_x is the distance between the centers of two adjacent elements. The angle of divergence can be found by the approximating equation (1):

$$\theta_a = \arctan \frac{D_{act}}{2F}. \tag{4}$$

Using the coordinates of the virtual element to calculate the delays used in the beamforming of the synthetic transmit aperture focusing leads to increased resolution.

The case, in which the virtual source is in front of the transducer (see Fig. 3) is met in all of the present imaging modalities, such as the linear array B-mode imaging. The beam before and after the focal point spreads out and the same region is insonified by several consecutive transmissions. The echos received by the same receive element from a given point at several consecutive emissions have almost the same amplitude, but different phases. Combining them can increase the resolution in transmit. This is practically a shift from a linear array to synthetic aperture imaging.

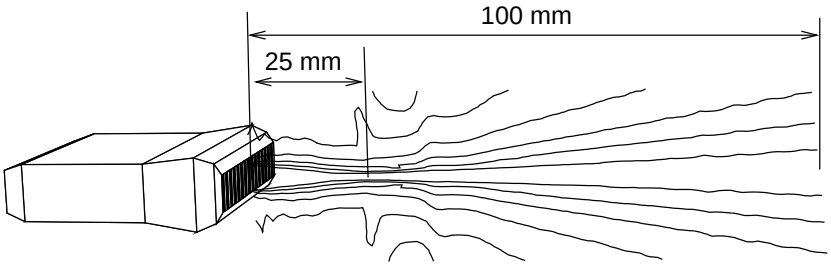

Figure 4. The beam profile of a a linear array transducer. The contours are shown at levels -6 dB apart, starting from -6 dB. The amplitude is normalized to the maximum at each depth.

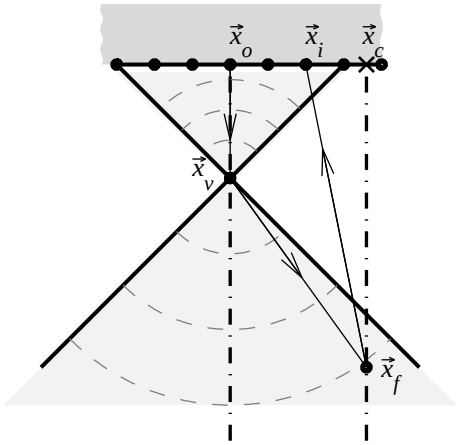

Figure 5. Pulse-echo path for the virtual source element in the azimuth plane.

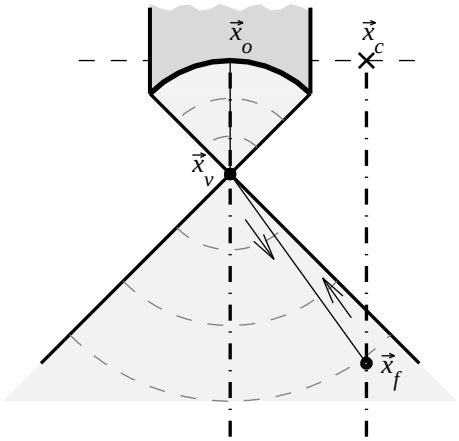

Figure 6. Pulse-echo path for the virtual source element in the elevation plane.

1.2 In the Elevation Plane

The linear array transducers can either be unfocused or focused in the elevation plane. The focusing is normally achieved with an acoustic lens, and is fixed. The pressure field is rather complicated. There exist, however, a couple of cases for which the field can be treated separately in the azimuth and elevation planes: the fixed transmit focus in the azimuth plane coincides with the fixed focus in the elevation plane, or the beam in the azimuth plane is dynamically focused.

A case of the pressure field in the elevation plane is shown in Fig. 4. The linear array transducer has a center frequency of 7.5 MHz and 60 % fractional bandwidth. The excitation is a 2-cycles Hanning weighted RF pulse at the center frequency. The height of the transducer is 4.5 mm and the elevation focus is at 25 mm from the transducer surface. The beam is dynamically focused in the azimuth plane. If this transducer is used to sweep a volume for 3D imaging, the resolution in the azimuth and elevation planes will differ greatly.

It is possible to use the fixed elevation focus as a virtual source *only* in the elevation plane and to post focus the already *beamformed* in the azimuth plane scan lines.[8] In this way the resolution in the elevation plane is increased and becomes comparable to the resolution in the azimuth plane.

The next section presents the various focusing schemes. It presents the synthetic transmit aperture focusing, and the monostatic synthetic aperture focusing. The exposition continues in Section 3 with the simulation and experimental investigation of the shape of the wavefront, and shows that it agrees with the aforementioned assumptions. Section 4 explores the increase in resolution and penetration depth by using the various focusing techniques. The paper finishes with a short discussion.

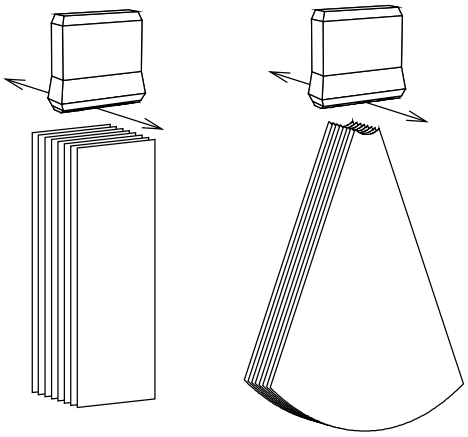

Figure 7. 3D scanning using a linear and a phased array.

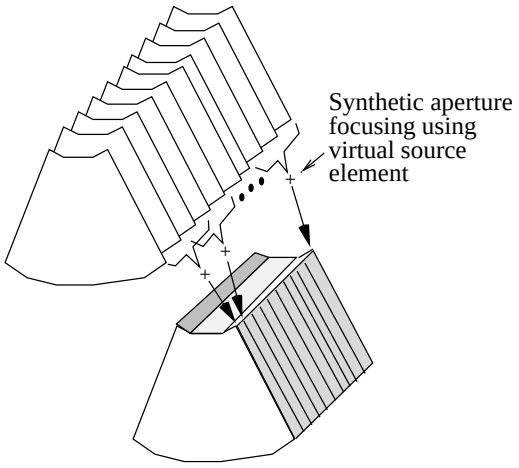

Figure 8. Post focusing in the elevation plane.

2. FOCUSING SCHEMES

Figure 5 shows the propagation path for a virtual source in the azimuth plane. In the case shown, the virtual source is in front of the transducer. The center of the active aperture is the element with coordinates $\vec{x}_o$, and is used as a reference point for calculating the delays in transmit. The pulses sent by the elements from the active aperture arrive at the transmit focus $\vec{x}_v$ at the same time instance. The wave then diverges. The shape of the wave front before and after $\vec{x}_v$ is shown with dashed arcs. The dashed-and-dotted line passing through $\vec{x}_c$ and $\vec{x}_f$ is the scan line being beamformed. The point $\vec{x}_f$ is the current focal point in receive, and $\vec{x}_c$ is the origin of the scan line.

The delay applied on the received element i, which has coordinates $\vec{x}_i$, when focusing at $\vec{x}_f$ is:

$$\tau_i = \frac{1}{c}\left(2|\vec{x}_f - \vec{x}_c| - (|\vec{x}_v - \vec{x}_o| + |\vec{x}_f - \vec{x}_v| + |\vec{x}_f - \vec{x}_i|)\right). \tag{5}$$

The delay is relative to the time t from the trigger of the transmission:

$$t = \frac{2|\vec{x}_f - \vec{x}_c|}{c}. \tag{6}$$

The notion of a delay with respect to a current time instance is used only for historical reasons. In fact, if the signal is stored in a computer memory, then only the pulse echo propagation time is necessary in order to reconstruct a point.

Figure 6 shows the beam-profile of a virtual source in the elevation plane. The elevation focus is at $\vec{x}_v$. The dashed-and-dotted line passing through the points $\vec{x}_c$ and $\vec{x}_f$ is the currently beamformed scan line. The delay applied on the received signal in order to beamform at $\vec{x}_f$ is:

$$\tau = \frac{2}{c}\left(|\vec{x}_f - \vec{x}_c| - (|\vec{x}_v - \vec{x}_o| + |\vec{x}_f - \vec{x}_v|)\right). \tag{7}$$

The delay τ is again relative to the time instance $t = 2|\vec{x}_f - \vec{x}_c|/c$.

In the case of 3D synthetic aperture imaging using a linear array, the beamformation procedure can be divided into two stages. In the first stage the volume is scanned plane by plane as shown in Fig. 7. The image in each plane is beamformed independently, by using (5) for the delay calculations. In the second part of the formation of the volume, the resolution in the elevation plane is increased by post focusing. From each plane, a scan line beamformed in the same direction is taken. The resulting set of RF lines are considered as signals acquired by transmitting and receiving with a single virtual source at different spatial locations. The final scan line in the

Parameter name	Notation	Value	Unit
Center frequency	f_0	7.0	MHz
Transducer pitch	d_x	208	μm
Element width	w	173	μm
Element height	h	4.5	mm
Elevation focus	F	25	mm

Table 1. Parameters of the used transducer array.

volume is obtained by beamforming these RF lines using synthetic aperture focusing. The delays are calculated by (7).

All of the presented focusing schemes rely on the assumption that within some limits, the created wavefront is a part of a cylindrical/spherical wave. Before exploring the increase in resolution in Section 4, the shape of the wavefront will be investigated in the next section.

3. THE WAVEFRONT OF THE VIRTUAL SOURCE

The shape of the radiated wave front is investigated through simulations and measurements to find how closely it approximates a spherical wave. Figure 9 shows the simulated field of a focused linear array. The points at which the field was simulated are placed in a polar coordinate system, with the focal point being the center. The simulations were done using the program FIELD II.[9] The simulation parameters are chosen such as the parameters of the linear array transducer, and are given in Table 1. The number of active elements is $N_{act} = 64$, and the virtual source in the azimuth plane is located 25 mm below the transducer. The thick lines in the plots show the estimated divergence angle θ_a:

$$\theta_a = \arctan \frac{N_{act} d_x}{2F} = \arctan \frac{11.07 \text{ [mm]}}{25 \text{ [mm]}} \approx 12.4^\circ \tag{8}$$

Figure 10 shows the simulated wavefront for the same transducer, but for the case when the virtual source is located behind the transducer. The pressure field is again calculated along an arc. The fact that within the angle of divergence the phases are aligned, means that the wave-front is circular/spherical.

This hypothesis was also verified experimentally for the pulse-echo case. Figure 11 shows a spherical wavefront, at a distance r from the virtual source. The radius r of the wavefront can be found by:

$$r = \frac{\Delta z^2 + \Delta x^2}{2\Delta z} \tag{9}$$

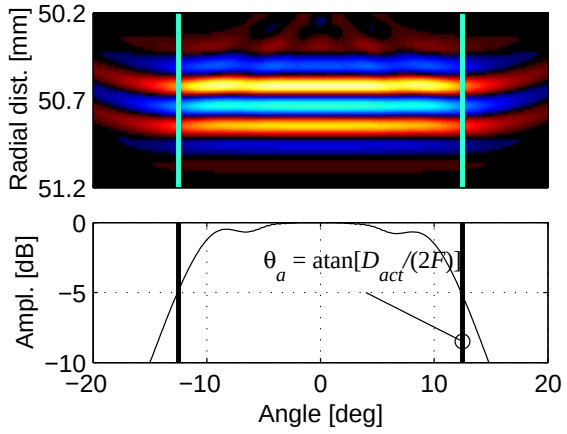

Figure 9. Simulated pressure field. The virtual source is in front of the transducer.

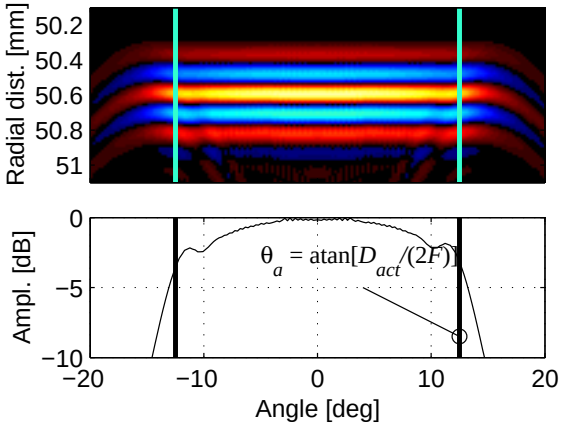

Figure 10. Simulated pressure field. The virtual source is behind the transducer.

where Δx and Δz are distances in lateral and axial directions. The difference in the pulse-echo propagation times from the virtual source to points A and C, and back is:

$$\Delta t = \frac{2\Delta z}{c}. \tag{10}$$

This gives a practical procedure to check whether the assumption for a virtual source element actually hold in a practical situation. An image of a single point is acquired using the same fixed focus, both in transmit and receive. The time shifts Δt between the RF lines at $\Delta x > 0$ and central RF line ($\Delta x = 0$) are found using cross-correlation. From the time shifts the radius r is estimated.

Figure 12 shows the result of such an experiment. A wire perpendicular to the azimuth plane and parallel to the transducer surface was scanned. 64 elements were used both in transmit and receive. The parameters of the transducer are the same as the ones shown in Table 1. The sampling frequency is $f_s = 40$ MHz. The wire was scanned using a fixed focus in transmit and receive. The theoretical curve was generated using the estimated radius. The figure shows that the wavefront of a focused transducer can be traced back to a single virtual source. This makes it possible to modify most of the existing beamformation techniques such as to use synthetic aperture focusing for increasing the resolution of the images.

4. INCREASE IN RESOLUTION

The use of virtual source elements for synthetic aperture imaging is well studied. Usually the virtual sources are created behind the transducer, and very few elements are used in transmit, typically between 7 and 30.[4–7] The error introduced by *not* taking into account the actual position of the virtual source, does not influence the focusing, and the created image is dynamically focused both in transmit and receive. The use of multiple elements in the synthetic aperture imaging is dictated due to the low signal to noise ratio. The more elements used, the better the SNR is. The use of more elements, however, makes it necessary to use the position of the virtual source element in the calculation of the focusing delays.

In the following it will be demonstrated that by taking into account the position of the virtual source, the dynamic transmit and receive focusing can be achieved even for large numbers of transmit elements.

4.1 Virtual Sources in the Azimuth Plane

The use of linear and phased arrays is usually confined to displaying a cross-sectional view of the human anatomy. The conventional scanners use a fixed focus in transmit and a dynamic focus in receive. Despite of the dynamic receive focusing, the image changes its appearance with depth as it can be seen from columns 1 and 3 of Fig. 13. The figure shows simulated B-mode images of a point scatterer positioned 100.5 mm in front of a transducer. The parameters of the transducer are given in Table 1*. The transmit focus is varied from 30 to 75 mm, and in receive dynamic focusing is used. The number of channels both in transmit and in receive is 128. The images

*All simulations and measurements in this paper have the same parameters, unless explicitly stated.

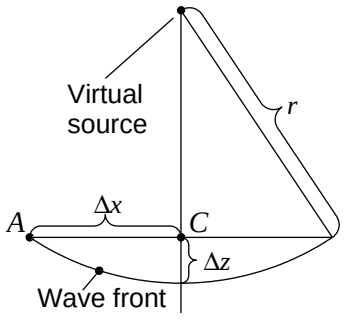

Figure 11. Geometry for estimation of the radius.

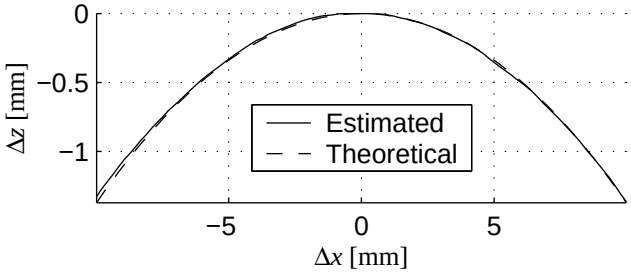

Figure 12. Estimated wave front compared with an ideal circular one.

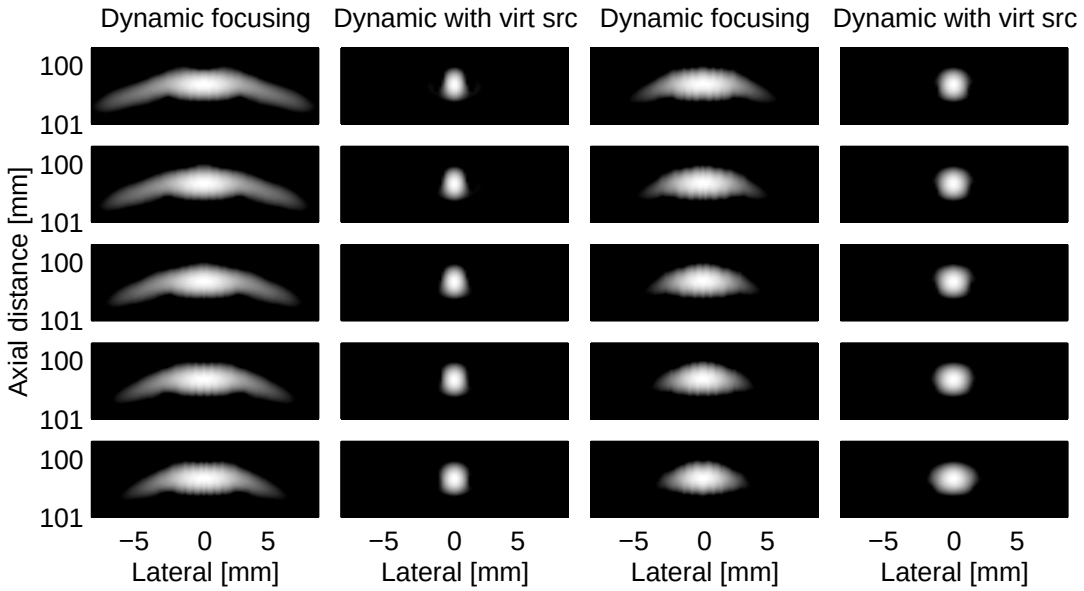

Figure 13. Simulated point spread functions. The transmit focus is varied between 30 mm and 75 mm at steps of 5 mm. In columns 1 and 3 the focusing in receive is dynamic. In columns 2 and 4 the dynamic receive focusing is combined with synthetic transmit aperture focusing based on a virtual source element.

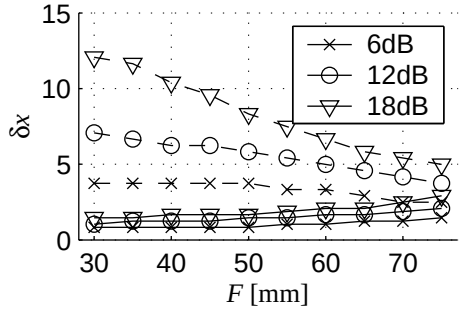

Figure 14. The size of measured PSF in the azimuth plane as a function of the transmit focus. The B-mode images of the PSFs are given in Fig. 13.

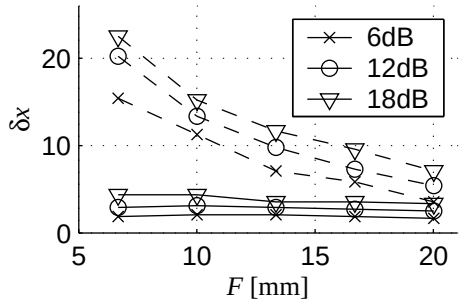

Figure 15. The size of measured PSF in the azimuth plane as a function of the transmit focus. The B-mode images of the PSFs are given in Fig. 16.

have a dynamic range of 40 dB. Using the same RF data, and applying synthetic transmit aperture focusing (STAF), the resolution of the image is increased as it can be seen from columns 2 and 4 of the same figure. The lateral size δx of the point spread function (PSF) does not vary significantly with the change of depth F of the transmit focus, as it can be seen from Fig. 14. In the figure the dashed lines are used for the PSF obtained with conventional dynamic focusing, and the solid lines are for the images formed with STAF.

Figure 15 shows the size of a measured point spread function. The measurements were done in a water bath. A steel wire, 0.1 mm in diameter, positioned 43 mm below the transducer surface was scanned for several depths of the transmit focus. Only 33 elements were used in transmit and 64 elements in receive. The measurements were done with the XTRA system, developed by Søren Kragh Jespersen for CADUS.[10] The B-mode images of the experiment are shown in Fig. 16. 192 emissions were performed. The lateral distance between the transmit focal points (virtual sources) was equal to the pitch of the transducer $d_x = 208\mu$m. Fixed focusing was used in receive. The *beamformed* lines were post-focused using monostatic synthetic aperture focusing (SAF). The delays were calculated using (7). From Fig. 16 it can be seen that using SAF also gives a lateral resolution which is independent of the depth of the transmit focus.

Finally, a tissue mimicking phantom was scanned with the experimental scanner RASMUS built by us at the Center for Fast Ultrasound Imaging.[11] The speed of sound was $c = 1540$ m/s, and the attenuation was 0.25 dB/(cm.MHz). A short pulse of 1 cycle was used in transmit. 128 channels were used both in transmit and receive. The transmit focus was set at 40 mm. The number of lines was 128, and the lateral distance between two adjacent virtual sources was 208 μm. The same RF signals were used to form a linear array B-mode image with dynamic receive focusing, and an image with synthetic transmit aperture focusing. Figure 17 shows the B-mode image beyond the transmit focus. The result reveals that the STAF image has a uniform resolution in depth. Even more, due to the use of *all* acquisitions to form each of the scan lines, the signal to noise ratio is significantly improved, and the penetration depth is increased. An example of this is the set of points at a depth of 100 mm, which are almost invisible in the conventional image.

To summarize, in this section it was verified through simulation and measurements that using synthetic aperture focusing based on virtual sources gives images that can be dynamically focused both in transmit and receive. After the beam has been focused, it can be treated as a signal sent, and received by a virtual source in the elevation plane.

4.2 Virtual Sources in the Elevation Plane

The considerations in this sections are for the case, in which a volume is scanned by a linear or phased array, which is moved in the elevation direction. At every position of the transducer, a B-mode image is formed using STAF with a virtual source in the azimuth plane. Then the beamformed RF scan lines are treated as signals sent and received by a single source. In this case, the source coincides with the fixed elevation focus. Figure 18 (top) shows the shape of the point spread function of the acquired volume. The surface is reconstructed at a level of -30 dB. The point is 70 mm below the surface of the transducer. Due to the STAF focusing, the size in the azimuth plane δx is much smaller than the size in the elevation plane δy. After synthetic aperture focusing is applied (the delays are calculated from (7)), δy becomes comparable with δx.[8] The PSF in Fig. 18 was simulated at steps $\Delta y = 0.5$ mm in elevation direction, which for this case is 1.75λ. The total number of positions was 95. The number beamformed scan lines used in the post beamforming was 40.

This algorithm was verified also experimentally. A point scatterer mounted in an agar block 96 mm away from the transducer was scanned. The step in the elevation direction was $\Delta y = 375$ μm. The diameter of the point scatterer was 100 μm. Figure 19 shows a contour plot of the cross-section of the PSF in the elevation plane. The contours are drawn at levels -6 dB apart, starting from -6 dB. The number of lines used in the SAF post focusing was 60. It can be seen that the -6 dB size of the PSF is reduced from 7 mm to less than 2 mm.

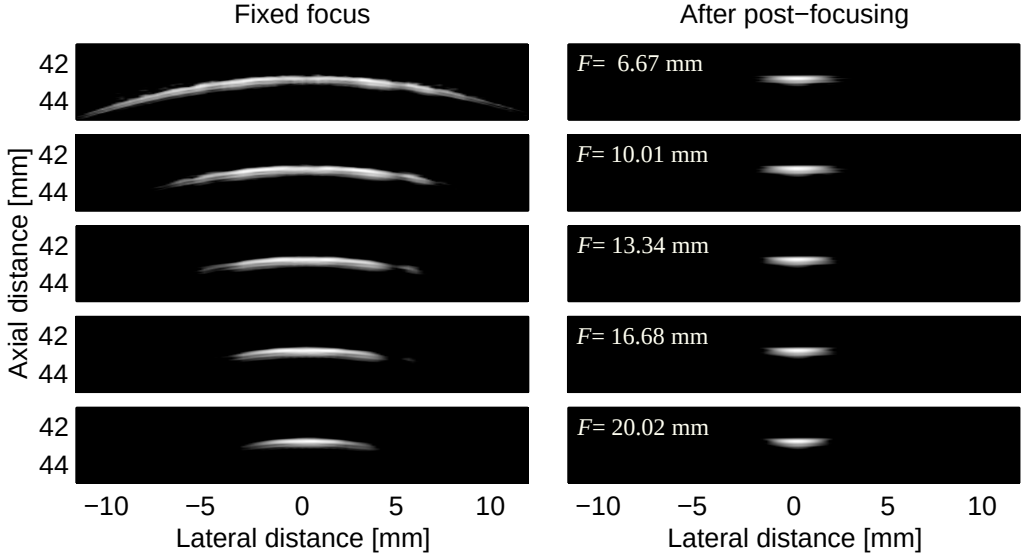

Figure 16. B-mode images of a wire in a water bath. The number of active elements is 33.

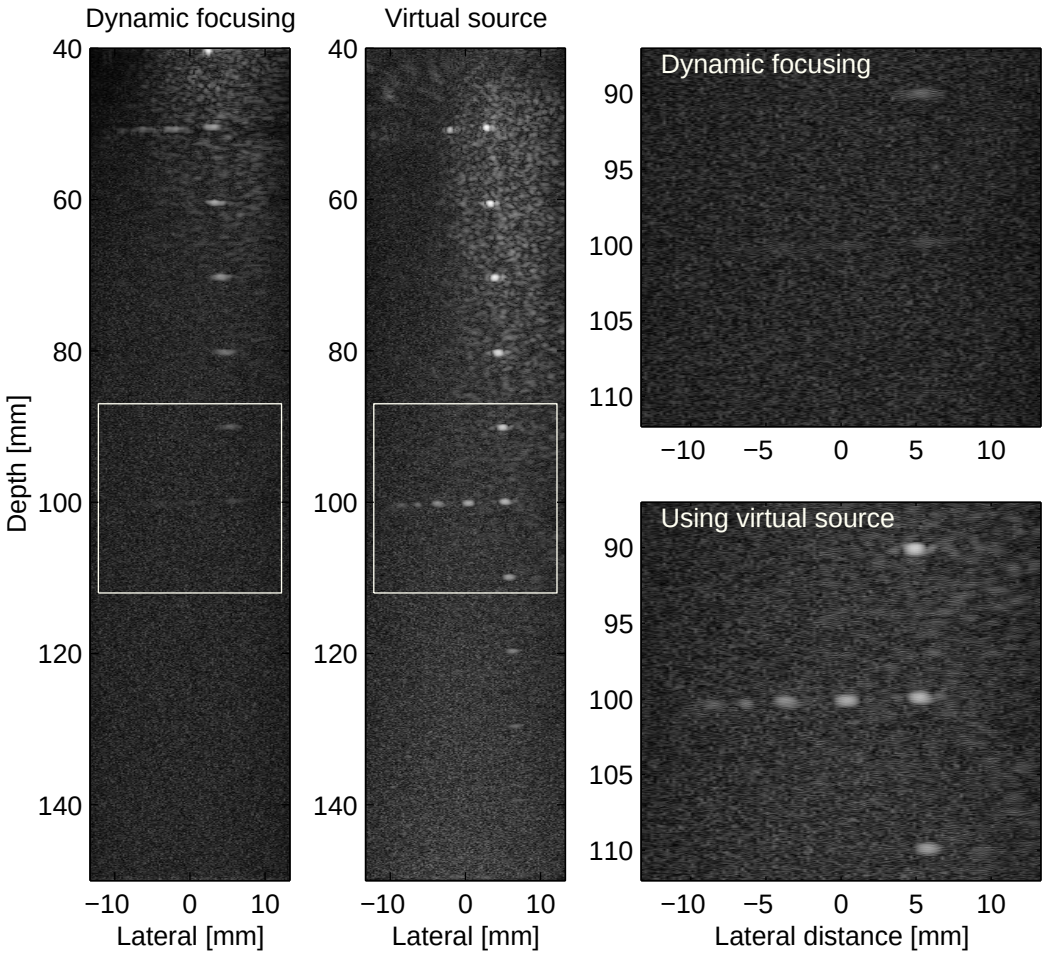

Figure 17. B-mode images of a tissue-mimicking phantom.

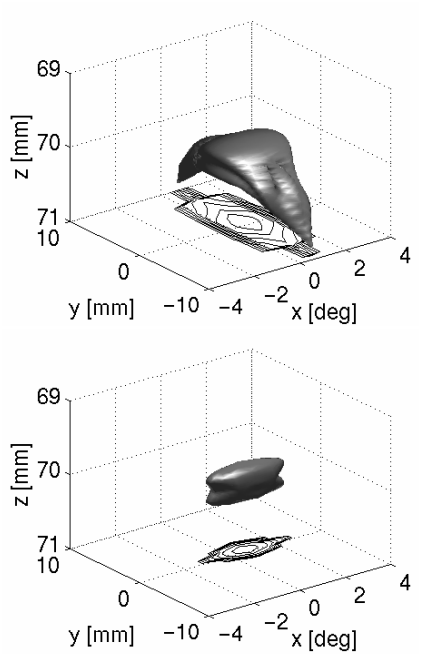

Figure 18. Simulated 3D point spread function: (top) before, and (bottom) after SAF post focusing in the elevation plane.

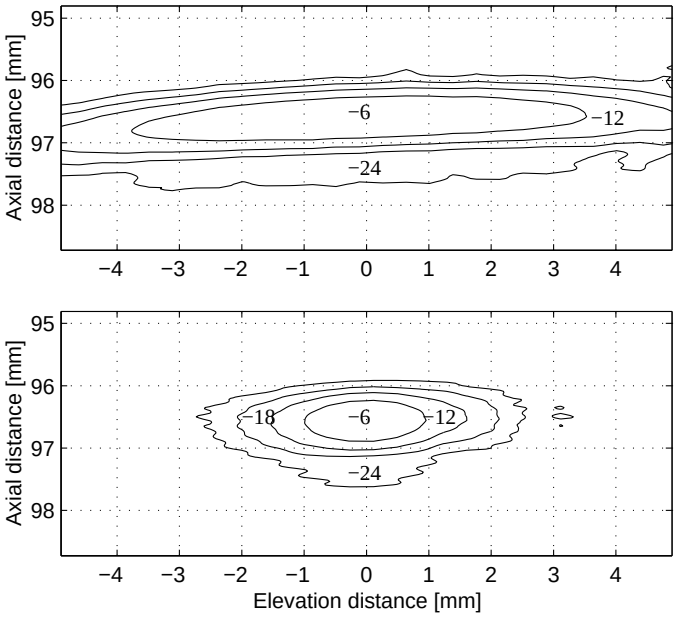

Figure 19. Cross section in the elevation plane of a measured point spread function. The numbers show the levels in the respective regions, i.e., the first contour delineates the -6 dB region.

5. CONCLUSIONS

This paper has suggested a framework for post focusing of ultrasound images based on the concept of the virtual source. The validity of the assumption that a virtual source exists, and that it creates a wave which is a part of a sphere/cylinder with certain limits, was verified through both simulations and pulse-echo measurement. It was also suggested that the focusing in the azimuth and elevation planes can be treated separately, and that the concept of virtual source can be used independently in the two planes. The simulations and measurements showed that the resolution in the azimuth plane can be increased, and be independent of the transmit focus depth. It was also shown that for the case of 3D scanning with a linear or phased array, the resolution in the elevation plane can be increased to match the one in the azimuth plane.

ACKNOWLEDGMENTS

This work was supported by grant 9700883 and 9700563 from the Danish Science Foundation and by B-K Medical A/S, Gentofte, Denmark.

REFERENCES

1. C. Passmann and H. Ermert. Adaptive 150 MHz ultasound imaging of the skin and the eye using an optimal combination of short pulse mode and pulse compression mode. In *Proc. IEEE Ultrason. Symp.*, pages 1291–1294, 1995.
2. C. Passmann and H. Ermert. A 100-MHz ultrasound imaging system for dermatologic and ophthalmologic diagnostics. *IEEE Trans. Ultrason., Ferroelec., Freq. Contr.*, 43:545–552, 1996.
3. C. H. Frazier and W. D. O'Brien. Synthetic aperture techniques with a virtual source element. *IEEE Trans. Ultrason., Ferroelec., Freq. Contr.*, 45:196–207, 1998.
4. M. Karaman, P. C. Li, and M. O'Donnell. Synthetic aperture imaging for small scale systems. *IEEE Trans. Ultrason., Ferroelec., Freq. Contr.*, 42:429–442, 1995.

5. G. R. Lockwood, J. R. Talman, and S. S. Brunke. Real-time 3-D ultrasound imaging using sparse synthetic aperture beamforming. *IEEE Trans. Ultrason., Ferroelec., Freq. Contr.*, 45:980–988, 1998.
6. S. I. Nikolov, K. Gammelmark, and J. A. Jensen. Recursive ultrasound imaging. In *Proc. IEEE Ultrason. Symp.*, volume 2, pages 1621–1625, 1999.
7. S. I. Nikolov. *Synthetic Aperture Tissue and Flow Ultrasound Imaging.* PhD thesis, Ørsted•DTU, Technical University of Denmark, 2800, Lyngby, Denmark, 2001.
8. S. I. Nikolov and J. A. Jensen. 3D synthetic aperture imaging using a virtual source element in the elevation plane. In *Proc. IEEE Ultrason. Symp.*, volume 2, pages 1743–1747, 2000.
9. J. A. Jensen. Field: A program for simulating ultrasound systems. *Med. Biol. Eng. Comp.*, 10th Nordic-Baltic Conference on Biomedical Imaging, Vol. 4, Supplement 1, Part 1:351–353, 1996b.
10. S. K. Jespersen, J. E. Wilhjelm, and H. Sillesen. Multi-angle compound imaging. *Ultrason. Imaging*, 20:81–102, 1998.
11. J. A. Jensen, O. Holm, L. J. Jensen, H. Bendsen, H. M. Pedersen, K. Salomonsen, J. Hansen, and S. Nikolov. Experimental ultrasound system for real-time synthetic imaging. In *Proc. IEEE Ultrason. Symp.*, volume 2, pages 1595–1599, 1999.